



Coulomb blockade and quantum confinement in field electron emission from heterostructured nanotips

Victor I. Kleshch ^{1,*}, Vitali Porshyn,² Dirk Lützenkirchen-Hecht,² and Alexander N. Obraztsov ^{1,3}

¹*Department of Physics, Lomonosov Moscow State University, Moscow 119991, Russia*

²*Physics Department, Faculty of Mathematics and Natural Sciences, University of Wuppertal, Wuppertal 42119, Germany*

³*Department of Physics and Mathematics, University of Eastern Finland, Joensuu 80101, Finland*



(Received 7 October 2020; revised 11 December 2020; accepted 18 December 2020; published 31 December 2020)

An electron field emission (FE) mechanism, which includes Coulomb blockade and quantum confinement effects, is revealed for heterostructured emitters composed of quantum dots and nanowires self-assembled at diamond nanotips. The total energy distributions of the emitted electrons show multiple peaks attributed to the discrete electronic states of the quantum-confined emitter with the corresponding energy levels oscillating as a function of the applied voltage due to the Coulomb blockade. The FE current-voltage characteristics exhibit a modified Coulomb staircase with additional steps becoming more pronounced with increasing voltage. The experimentally observed behavior is consistent with numerical simulations based on the model of Coulomb blockade in quantum dots in combination with the theory of FE from sharp tips.

DOI: [10.1103/PhysRevB.102.235437](https://doi.org/10.1103/PhysRevB.102.235437)

I. INTRODUCTION

The Coulomb blockade (CB) and quantum confinement effects in nanoscale heterostructures make it possible to manipulate individual electrons providing a platform for fundamental studies in quantum coherent electronics [1] and metrology [2]. In solid-state heterostructures, e.g., in a two-terminal system consisting of a nanostructure electrically isolated from the source and drain leads by tunnel junctions, potential barrier profiles are usually insensitive to the number N of electrons determining the charge Ne of the nanostructure. However, this is not the case in a vacuum electronic device based on field emission (FE) where the barrier between the nanostructure and the drain (anode) has a triangular shape which depends on the field strength proportional to N . This alters the physics of charge transport and allows observations of single-electron charging effects in FE, such as a Coulomb staircase in the current-voltage characteristics, under conditions which cannot be realized in solid-state devices [3].

Several experimental observations of FE from individual nanostructures [4–6] and molecules [7] in the single-electron regime have been reported over the last decade. The most remarkable behavior (in comparison to solid-state devices) was observed for nanostructures attached to a needle-shaped cathode and located at a macroscopic distance from the anode. In particular, the Coulomb staircase was observed for temperatures of up to 1000 K, operating currents up to several microamperes, and voltages, necessary to transfer an extra electron to the nanostructure, of few hundreds of volts [4,6]. In these pioneering experiments single-electron charging was observed for carbon nanotubes and nanowires where quantum confinement effects are small and are not manifested in FE.

In this paper we make the next step by exploring FE in heterostructures based on small-size quantum-confined carbon nanowires. The heterostructures were created by modification of the atomic structure of the diamond needlelike crystallites caused by the action of a strong electric field and Joule heating during FE [6]. First, we describe the main stages of this FE-induced reconstruction process, as shown in Fig. 1.

Initially, at low FE currents, nanoscale structures are formed at the apex of a pristine (unmodified) diamond nanotip due to the electric field-assisted diffusion of surface atoms. Self-organization of such kind of nanostructures is a well-known phenomenon in FE from uncleaned emitters, e.g., carbon nanotubes [8,9], graphene [10], tungsten tips [11,12] and Spindt cathodes [13]. In this case, electrons tunnel into the vacuum through discrete energy states [separated by a characteristic energy $\Delta\epsilon$; see Fig. 1(a)] arising due to the quantum confinement in the nanostructure, which can therefore be referred to as a quantum dot (QD).

At high FE currents, QDs evaporate, and the surface diamond layer with a few-nanometer thickness transforms into amorphous carbon (a -C). After that, electron emission is typically governed by the classical Fowler-Nordheim (FN) mechanism [14,15] [Fig. 1(b)]. Furthermore, elongated carbon nanostructures (nanowires) with a length of about 10 nm can be formed by varying the electric field and FE current as directly observed by transmission electron microscopy (TEM) [6]. The quantum confinement is small and has no effect on FE in such nanowires. However, since the nanowire is electrically isolated from the underlying a -C layer by a potential barrier, the CB of the FE current [characterized by the charging energy $\delta\epsilon$; see Fig. 1(c)] becomes observable. The potential barrier between the nanowire and a -C layer is formed due to the difference in sp^2 -hybridized carbon content. The current density flowing through the nanowire during its formation is at least $1 \mu\text{A}/\text{nm}^2$ [6]. Joule heating corresponding to this

*Corresponding author: klesch@polly.phys.msu.ru

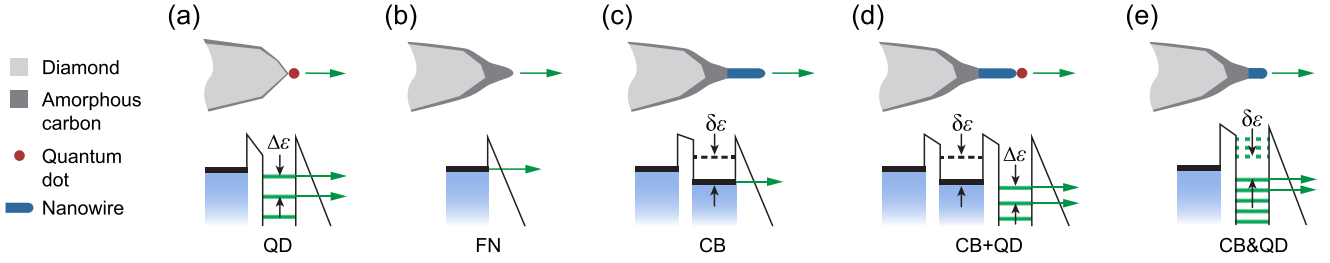


FIG. 1. (a)–(e) Schematic illustration of the emitter and corresponding energy diagrams at different stages of the FE-induced structure modification. See text for details.

value is high enough for its crystallization into graphitic layers with sp^2 hybridization, as was shown, for example, by the *in situ* TEM experiments [16,17]. At the same time, the current density through the relatively thick a -C layer located underneath the nanowire is smaller and, therefore, the content of sp^2 -carbon in this region is lower.

Finally, one can imagine a structure where the CB and quantum confinement coexist. In the case of QD structure formation directly at the apex of a nanowire, a double-well structure is formed [Fig. 1(d)], and single-electron charging and energy-quantization effects act independently on charge transport. Also, the electron quantum confinement is possible in the nanowire itself [Fig. 1(e)], when its length is sufficiently small, i.e., when it is comparable to the de Broglie wavelength. In this case, an interplay between the CB and quantum confinement may be observed since both effects coexist in one and the same structure.

In this paper, we demonstrate that all transport regimes shown in Fig. 1 are observed experimentally for diamond nanotip emitters. In our previous work [6], we investigated in detail the pure CB regime and developed a model that is in excellent agreement with experiment. Here, we present a generalized model for the CB&QD regime (Sec. II), perform a comparative analysis of the experimental data obtained in different transport regimes (Sec. III), and draw a brief conclusion (Sec. IV).

II. MODEL

In order to model the charge transport in a double-barrier structure with a quantum confined nanowire [Fig. 1(e)], it is straightforward to use the master equation [3,18], which allows the determination of the probabilities P_N of finding the nanowire in the state with N electrons at a fixed voltage. In the stationary case, it can be written as

$$P_N \sum_k \left(\Gamma_k [1 - f(\varepsilon_k + \Delta U_N)] g_N(\varepsilon_k) + \frac{I_{FE}(\varepsilon_k, F_N)}{e} \right) = P_{N-1} \sum_k \Gamma_k [1 - g_N(\varepsilon_k)] f(\varepsilon_k + \Delta U_N). \quad (1)$$

Here the sums on the left and right sides describe the total tunneling rates from and to the nanowire discrete energy levels ε_k , respectively. Each tunneling event is associated with a change in the Coulomb energy $\Delta U_N = U_N - U_{N-1} = (e^2/C)[N - 1/2 - C_A V/e]$, where C is the total capacitance of the nanowire, and C_A is the nanowire capacitance

with respect to the anode electrode. The function $f(\varepsilon) = 1/[1 + \exp(\varepsilon/k_B T)]$ is the Fermi distribution, $g_N(\varepsilon_k)$ is the electron distribution function in the nanowire, and $I_{FE}(\varepsilon_k, F_N)$ is the partial FE current from the energy level ε_k at an electric field $F_N = \alpha_V V + \alpha_N N$, where α_V and α_N are parameters determined by the geometry of the nanowire and surrounding electrodes. The solution of Eq. (1) gives the probabilities distribution P_N . The total FE current can then be calculated as a sum over all partial currents $I = \sum_N \sum_k I_{FE}(\varepsilon_k, F_N) P_N$.

FE current density for the case of emission from a free-electron gas is given by the standard Young formula [15]

$$j(\varepsilon, F) = \frac{j_0(F)}{d(F)} \frac{e^{\varepsilon/d(F)}}{1 + e^{\varepsilon/k_B T}}. \quad (2)$$

Here ε is the kinetic electron energy relative to the Fermi level, F is the electric field, j_0 is the total current density at $T = 0$ K given by $j_0(F) = A F^2 \exp(-B/F)$ (A/m^2), $d(F) = 9.76 \times 10^{-11} F \varphi^{-1/2} t^{-1}(y)$ (eV), $A = 1.54 \times 10^{-6} \varphi^{-1} t^{-2}(y)$, $B = 6.831 \times 10^{-9} \varphi^{3/2} v(y)$, $v(y)$ and $t(y)$ are tabulated functions of the variable $y = 3.7495 \times 10^{-5} F^{1/2}/\varphi$, F is in V/m, φ is in eV. The work function was set to $\varphi = 5$ eV, which is a typical value for graphite.

In the case of weak confinement, i.e., when the distance between neighboring levels ε_k is much less than $k_B T$, summation over k in Eq. (1) gives [19]

$$P_N \left[\frac{\Delta U_N}{e^2 R_T [1 - \exp(-\Delta U_N/k_B T)]} + \frac{I_{FE}(F_N)}{e} \right] = P_{N-1} \frac{\Delta U_N}{e^2 R_T [\exp(\Delta U_N/k_B T) - 1]}, \quad (3)$$

where R_T is the tunneling resistance. This equation describes the pure CB regime and was considered earlier [3,6].

III. RESULTS AND DISCUSSION

The FE experiments were carried out at room temperature in an ultrahigh vacuum setup using a diode configuration with a planar metal mesh anode and a cathode consisting of a diamond needle attached to a tungsten support tip. The DC voltage V was applied between the electrodes. The total FE current I was measured by a picoammeter, and the spectrum (total electron energy distribution) $J(\varepsilon)$ was measured by an electron spectrometer with a hemispherical analyzer located behind the mesh anode. The experimental details can be found elsewhere [6,20].

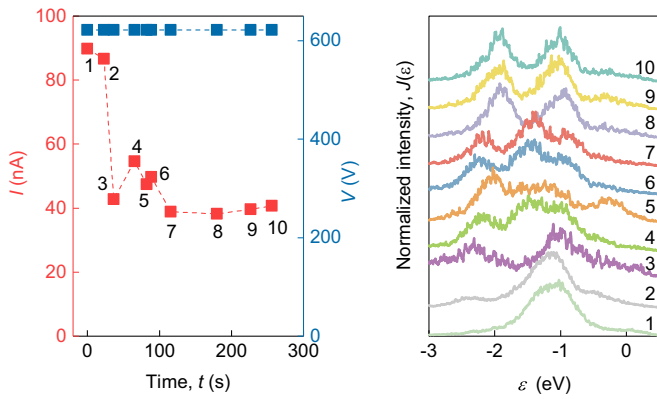


FIG. 2. Dependence of the FE current on time and the corresponding energy spectra at a fixed voltage, demonstrating the stabilization of FE from a pristine diamond needle.

A set of representative measurements for one of the diamond needles demonstrating the QD, FN, CB, and CB+QD

regimes (see Fig. 1) are presented in Secs. III A–III D, respectively. The CB&QD regime is demonstrated for another diamond-needle sample in Sec. III E.

A. FE from pristine diamond needle (QD regime)

FE from a pristine diamond needle occurred in the presence of self-assembled QD nanostructures [Fig. 1(a)], which caused strong instabilities of the FE current in initial measurements. By increasing the current to about 100 nA the nanostructures and electron emission become relatively stable, as shown in Fig. 2. An example of well reproducible measurements obtained after stabilization is shown in Fig. 3(a), where we present the dependence of $J(\epsilon)$ on V , the corresponding $I(V)$ curve, and the position of the energy peaks, $\epsilon_{\text{peak}}(V)$, for each $J(\epsilon)$ curve. The spectrum contains two well-separated peaks, which linearly shift with V . Moreover, a third peak appears at high V . This behavior is in good agreement with the FE model involving localized states of a self-assembled QD structure [Fig. 1(a)]. The energy peaks

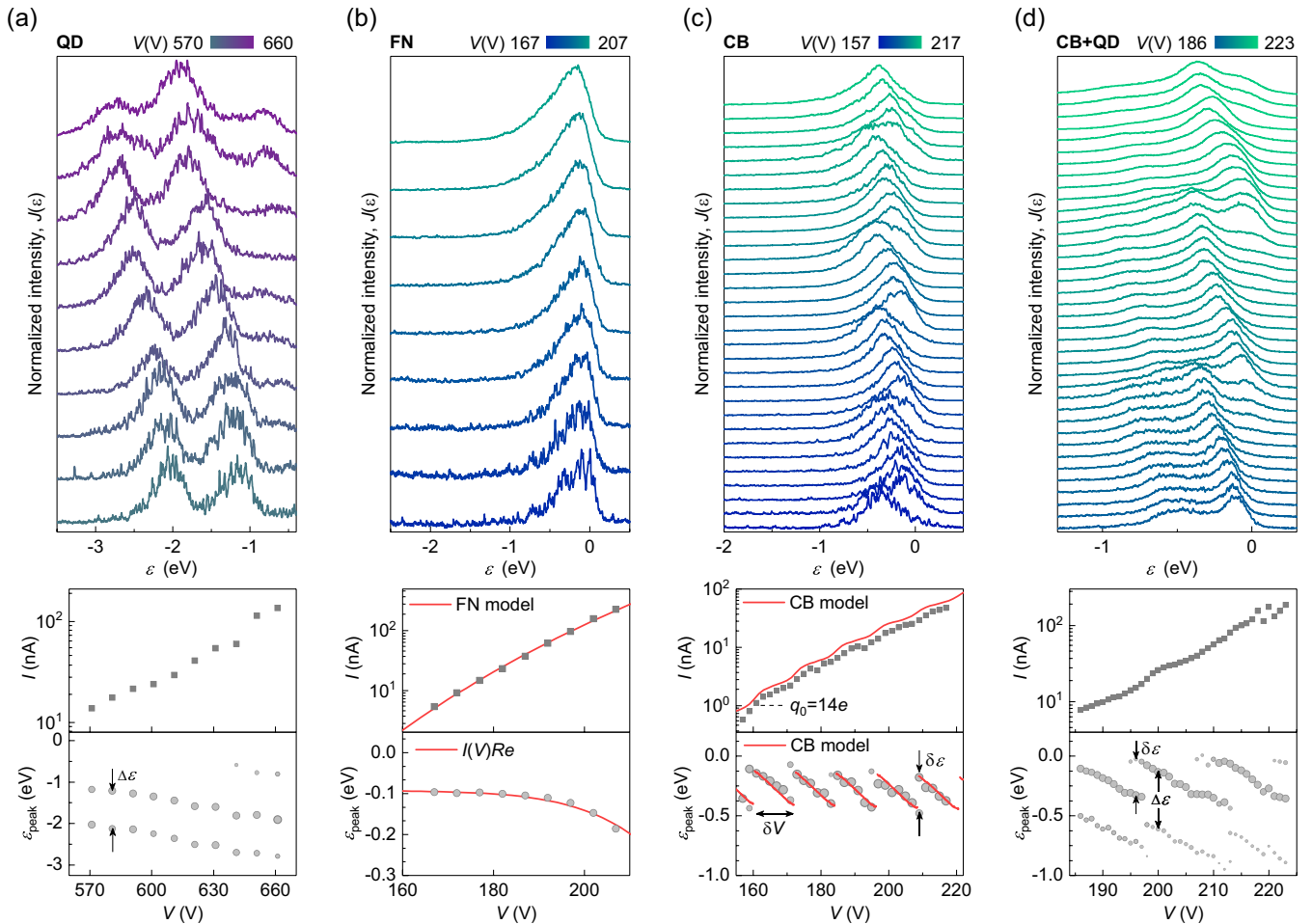


FIG. 3. (a)–(d) $J(\epsilon)$, I , and ϵ_{peak} as a functions of V , measured at different stages of the FE-induced reconstruction shown in Figs. 1(a)–(d), correspondingly. Each $J(\epsilon)$ curve is normalized to unity. The size of each point in $\epsilon_{\text{peak}}(V)$ is proportional to the amplitude of the energy peak, obtained by $J(\epsilon)$ curve fitting as described in Supplemental Material [22]. The red lines in (b) are the $I(V)$ curve fit by the FN equation with $a = 5960 \text{ nA/V}^2$, $b = 2890 \text{ V}$, and fit of the shift in $\epsilon_{\text{peak}}(V)$ with $R = 400 \text{ k}\Omega$. The red lines in (c) are fits of $I(V)$ and $\epsilon_{\text{peak}}(V)$ obtained by solving Eq. (3) with parameters $C_A = 13.5 \times 10^{-21} \text{ F}$, $C = 5.1 \times 10^{-19} \text{ F}$, $R_T = 200 \text{ k}\Omega$, $\alpha_V = 5.9 \times 10^7 \text{ m}^{-1}$, $\alpha_N = 5.6 \times 10^8 \text{ V/m}$, $T = 300 \text{ K}$. The $I(V)$ curve fit is shifted for clarity.

correspond to discrete energy states shifting with voltage due to penetration of the electric field into the QD [12,21].

B. FE from clean *a*-C surface (FN regime)

A substantial structural modification of the diamond nanotip, formation of an *a*-C layer, and removal of QD structures were initiated after the FE current increase above 1 μ A. A common FN emission behavior [Fig. 1(b)] was revealed for clean *a*-C surface, as shown in Fig. 3(b). In this case, the spectrum consists of a single asymmetric peak which shifts nonlinearly with V due to the voltage drop, IR , developed across the emitter having an electrical resistance R . The FE current follows the standard FN equation $I(V) = aV^2 \exp(-b/V)$, where a and b are fitting parameters.

C. FE from nanowire (CB regime)

When a carbon nanowire was formed at the top of the *a*-C layer, the FE was governed by the CB effect [Fig. 1(c)]. As a result, a periodic modulation (Coulomb staircase) in the $I(V)$ curve and sawtooth oscillations in the $\varepsilon_{\text{peak}}(V)$ dependence are observed [Fig. 3(c)]. The amplitude of $\varepsilon_{\text{peak}}(V)$ oscillations gives the charging energy, which is determined by the total capacitance of the nanowire, C , as $\delta\varepsilon = e^2/C$. The period of the oscillations is determined by the nanowire capacitance with respect to the anode electrode C_A as $\delta V = e/C_A$. The model of FE in the CB regime developed in Ref. [6] and based on Eq. (3) reproduces well the experimental data, as shown by the red lines in Fig. 3(c). The values of the obtained fitting parameters are within the limits determined in the previous work [6], where the relationship of these parameters with the structural and electronic characteristics of the emitter is considered in detail.

Thus, the CB effect observed for nanowires and the quantum confinement effect observed for QD structures manifest themselves differently in FE, and by measuring the energy spectra, one can unambiguously distinguish between them. Moreover, the spectral features, which are specific to each effect, can appear simultaneously, when a QD structure is formed at the apex of a nanowire.

D. FE from QD on nanowire (CB+QD regime)

Similar to the case of pristine diamond needles, QD structures can sometimes be formed during FE from nanowires, since adsorption layers accumulate over time even in ultrahigh-vacuum conditions [9]. An example of the spectrum structure transformation from a single peak to multiple peak as a result of the QD formation is shown in Fig. 4. It is worth noting that the FE characteristics of QD structures become unstable at currents above 100 nA, as can be seen in the $I(V)$ curve in Fig. 3(d). With a further increase in the current, QDs are completely removed, while the nanowires can remain stable up to currents of several microamperes [6].

We found that after the QD formation, simultaneous sawtooth oscillations were revealed for two well-separated energy peaks, spaced by $\Delta\varepsilon$. It should be noted that the $I(V)$ curve in Fig. 3(d) has a much steeper slope than in Fig. 3(c), and the current I is more than twice higher in the high- V region. At the same time, the period δV and amplitude $\delta\varepsilon$ of the

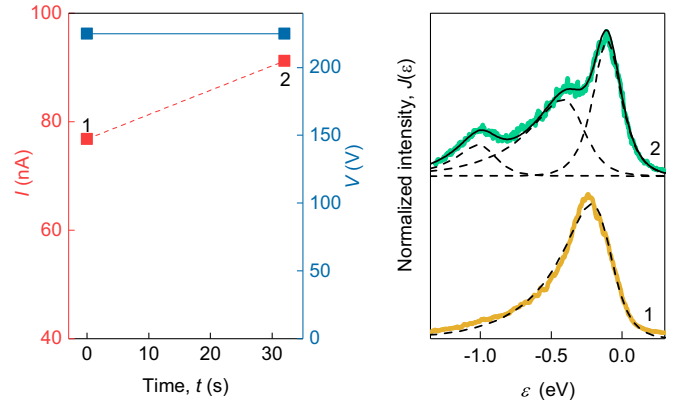


FIG. 4. Two successive measurements of FE current and electron spectrum at a fixed voltage, demonstrating the formation of a QD at the top of the nanowire. These measurements were performed between the measurements shown in Figs. 3(c) and 3(d). The dashed black lines are the fits of individual peaks in the spectra. The solid black line is the fit of the spectrum 2, which consists of three distinct peaks.

oscillations are almost the same. This can be well explained within the model shown in Fig. 1(d), where electrons tunnel into the QD from the nanowire Fermi level, which oscillates with V due to CB. Since the QD is much smaller in size as compared to the nanowire, the capacitances C and C_A , which determine $\delta\varepsilon$ and δV , did not vary significantly after the QD formation. However, the profile of the triangular barrier and the FE mechanism can be very different in the presence of QD, which explains the observed changes in the $I(V)$ curve.

E. FE from small-size nanowire (CB&QD regime)

Next, we consider the case of FE from the small-size nanowires [Fig. 1(e)], where quantum confinement is significant and can be observed experimentally. The size of a nanowire can be estimated from experimental data by extrapolating the CB oscillations to $V = 0$ V, which gives its characteristic charge q_0 as a ratio $q_0 \approx V_0/\delta V$, where V_0 is the voltage corresponding to the FE current I_0 . For example, in Fig. 3(c) $q_0 \sim 14e$ (at $I_0 = 1$ nA). We found that the evidence for quantum confinement effects appear at twice smaller q_0 values, as demonstrated in Figs. 5(a) and 5(b) for a sample with $q_0 \sim 7e$. It should be noted that in this case, limitations in the spectroscopy resolution did not allow us to resolve discrete energy peaks, as in the case of QDs, because of the smaller value of $\Delta\varepsilon$. Nevertheless, the current-voltage measurements revealed a well-reproducible short-period modulation of the current amplitude in the Coulomb staircase [Fig. 5(a)]. This is clearly visible in the normalized differential conductance dependence $(dI/dV)/(I/V)$, presented in Fig. 5(b), where high-amplitude peaks spaced by $\delta V \sim 25$ V are superimposed by less intense peaks with about threefold smaller spacing. This behavior resembles the modified Coulomb staircases observed in the transport through solid-state semiconducting QDs with strong asymmetry in the barriers, where discrete states and single-electron charging coexist [23,24]. However, in our case, the underlying physics is quite different due to

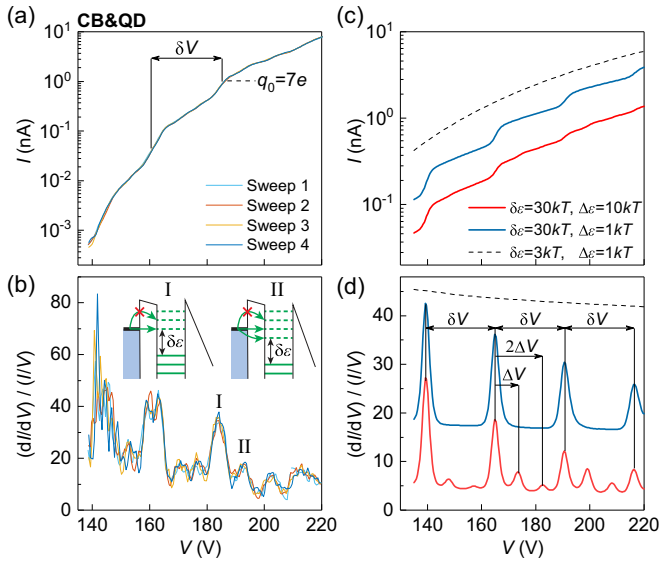


FIG. 5. (a) Experimental $I(V)$ characteristics and (b) the corresponding normalized differential conductance curves for a small nanowire. Insets in (b) show schematic diagrams of electron tunneling. (c), (d) Results of the simulations using Eq. (1) performed at $T = 300$ K for different $\delta\varepsilon$ and $\Delta\varepsilon$ with parameters $C_A = 6.3 \times 10^{-21}$ F, $C = 2 \times 10^{-19}$ F, $\Gamma_0 = 4.8 \times 10^9$ s $^{-1}$, $k_j = 1.3 \times 10^{-19}$ cm 2 , $\alpha_V = 4.5 \times 10^7$ m $^{-1}$, $\alpha_N = 8.2 \times 10^8$ V/m.

the voltage-dependent resistance of the emission barrier and completely different geometry of the experiment.

Good qualitative agreement between the simulation using Eq. (1) and experiment was obtained even in the simplest case of equidistant energy levels $\varepsilon_k = k\Delta\varepsilon$ populated according to the Fermi distribution $g_n(\varepsilon_k) = f(\varepsilon_k)$, constant tunneling rates $\Gamma_k = \Gamma_0 = \text{const}$, and partial FE currents given by $I_{\text{FE}}(\varepsilon_k, F_N) = k_j \Delta\varepsilon j(\varepsilon_k, F_N)$, where $j(\varepsilon_k, F_N)$ is defined by Eq. (2) and k_j is the pre-exponential factor, which is associated with the emission area, geometry, and the electronic properties of the emitter.

It should be noted that Eq. (2) is valid for FE from a flat surface and can lead to an overestimation of the FE current values by several orders of magnitude for emitters with a nanoscale radius of curvature [25]. Therefore, in order to match the experimental values of the FE current in simulation, the values of some fitting parameters had to be chosen physically incorrect, i.e., in contradiction to the physical properties of the nanoscale emitter. In particular, the obtained value of the parameter $k_j = 1.3 \times 10^{-19}$ cm 2 , which is mostly determined by the emission surface area, is much lower in comparison with the estimation of emission area S of a nanowire with characteristic radius $r \sim 1$ nm, $S \sim 2\pi r^2 \sim 10^{-15}$ cm $^2 \gg k_j$. Nonetheless, we used Eq. (2) to simulate the behavior of the current in the most general case, since the exact atomic and electronic structure of the confined nanowire is not known, and, therefore, the model can give only qualitative agreement with experiment.

When the thermal energy kT is substantially smaller than both energies $\delta\varepsilon$, $\Delta\varepsilon$, the simulated $I(V)$ curve [red line in Fig. 5(c)] has the staircase shape with an additional modulation that best matches the experiment when $\delta\varepsilon/\Delta\varepsilon \sim 3$.

The differential conductance curve exhibits high-amplitude periodic peaks, spaced by δV , and additional peaks shifted by an integer number of $\Delta V = (\Delta\varepsilon/\delta\varepsilon)\delta V$ from each main peak [Fig. 5(d)]. In the low- V region, the additional peaks are small, and the differential conductance curve is close to the blue curve simulated at $\Delta\varepsilon \sim kT$, i.e., in the classical CB regime. In the high- V region, amplitudes of the main and additional peaks become comparable.

The physical mechanism underlying the conductance behavior is explained schematically in the inset in Fig. 5(b). Scheme I corresponds to the main peak in the differential conductance, when just one energy level, that is aligned with the Fermi level in the electron reservoir, is available for tunneling into the nanowire. The levels shift downward with increasing V , due to the change in the Coulomb energy ΔU_N . When the second level aligns with the Fermi level of the reservoir (scheme II), the tunneling probability through the inner barrier (between the reservoir and the nanowire) sharply increases and an additional peak in the differential conductance is observed. With a further increase in V , the third level becomes allowed for tunneling, and so on, until the total energy shift reaches $\delta\varepsilon$ and another main peak appears. At low V , the additional peaks are weak, since the electron transport is determined by a less transparent outer (triangular) barrier, which depends only on the number of electrons on the nanowire and does not depend on the number of levels available for tunneling. The additional peaks increase with increasing V , because the inner barrier becomes a bottleneck for transport. At high V , the oscillations are washed out and the differential conductance curve follows the dashed line in Fig. 5(d), which is simulated with an order of magnitude smaller $\delta\varepsilon$ and $\Delta\varepsilon$.

It is important to note that in the experiment the differential conductance peaks are not equidistant [Fig. 5(b)], i.e., δV and ΔV increase with V . This can be attributed to the change in capacitive characteristics of the nanowire (in particular C_A , since it defines δV) due to the semiconducting properties of the carbon emitter. Because of the limited carrier concentration, the electric field penetrates into the nanowire and the supporting a -C layer, and the capacitances decrease with increasing voltage. We obtained good agreement with the experimental peak positions by introducing a slight linear decrease in C_A of 12% into the model, as shown in Fig. 6.

Let us finally discuss the possible mechanisms of electron tunneling in the considered structures, namely coherent and sequential tunneling processes, which, in general, both contribute to the transport through double-barrier structures [26]. The dominant mechanism depends on the coupling between the reservoir and the emitting nanostructure [27,28]. The coupling strength can be characterized by the tunneling resistance R_T . In the case of FE from nanowires [Fig. 3(c)], the coupling is weak and $R_T \gg R_q$ [6], where $R_q = h/e^2 \sim 25.8$ k Ω is the resistance quantum (von Klitzing constant). Under these conditions, single-electron charging effects become important, and transport occurs via sequential tunneling events described by the master equation. In the case of QDs, the coupling is strong and coherent tunneling prevails, which is reflected by the multiplex structure of the spectra [Fig. 3(a)]. In the intermediate case of small nanowires, the sequential tunneling approximation is still valid and the CB theory is consistent with experiment (Figs. 5 and 6). However, the discrepancies

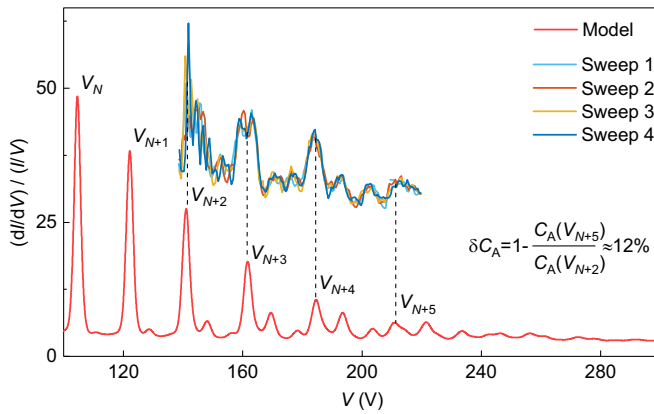


FIG. 6. Simulation of normalized differential conductance using Eq. (1) with $C_A(V) = C_{A0} - k_C V$, where $C_{A0} = 1.33 \times 10^{-20}$ F, $k_C = 1.82 \times 10^{-23}$ F/V. The other parameters are the same as in Fig. 5(d). The relative change of the C_A between voltages V_{N+2} and V_{N+5} is $\delta C_A \approx 12\%$. Experimental sweeps 1–4 are the same as in Fig. 5(b) and are shifted for clarity.

in the shape and amplitudes of the differential conductance peaks may indicate an additional contribution of coherent tunneling [28,29].

IV. CONCLUSION

In conclusion, we studied the combined effect of quantum confinement and single-electron charging in FE from

heterostructured nanotips composed of self-assembled carbon QDs and nanowires. The distinctive features, as compared to the typical properties of solid-state QDs, observed in the FE experiments, are explained by the strong dependence of the emission barrier transparency on the applied voltage and the charge of the self-assembled nanostructure, as well as by the peculiar geometry of vacuum FE devices, in which the source and drain are separated by a macroscopic distance. The observation of size and charge quantization effects at room temperature is possible in our experiments owing to the strong localization of a well-defined number of electrons in the carbon nanostructure and, at the same time, strong concentration of the electric field on its surface. This offers further opportunities for using the tip-shaped carbon heterostructures, e.g., in scanning QD microscopy [30] for probing local electrostatic potential fields and in laser-triggered single-electron sources [31–34] for low-energy electron holography [35] and ultrafast electron microscopy [36].

ACKNOWLEDGMENTS

Experimental and theoretical research was supported by Russian Science Foundation (Grant No. 19-72-10067). V.P. and D.L.-H. are grateful to German Federal Ministry of Education and Research (Project No. 05K13PX2) for infrastructure support. A.N.O. and V.I.K. are also grateful to the Academy of Finland (Grant No. 334552) for travel support.

V.I.K. performed the experiments and theoretical calculations, V.P. assisted with electron spectroscopy measurements, V.I.K., D.L.-H., and A.N.O. co-wrote the manuscript.

- [1] C. Bauerle, D. C. Glattli, T. Meunier, F. Portier, P. Roche, P. Roulleau, S. Takada, and X. Waintal, Coherent control of single electrons: a review of current progress, *Rep. Prog. Phys.* **81**, 056503 (2018).
- [2] J. P. Pekola, O. P. Saira, V. F. Maisi, A. Kemppinen, M. Mottonen, Y. A. Pashkin, and D. V. Averin, Single-electron current sources: toward a refined definition of the ampere, *Rev. Mod. Phys.* **85**, 1421 (2013).
- [3] O. E. Raichev, Coulomb blockade of field emission from nanoscale conductors, *Phys. Rev. B* **73**, 195328 (2006).
- [4] A. Pascale-Hamri, S. Perisanu, A. Derouet, C. Journet, P. Vincent, A. Ayari, and S. T. Purcell, Ultrashort Single-Wall Carbon Nanotubes Reveal Field-Emission Coulomb Blockade and Highest Electron-Source Brightness, *Phys. Rev. Lett.* **112**, 126805 (2014).
- [5] C. Kim, H. S. Kim, H. Qin, and R. H. Blick, Coulomb-controlled single electron field emission via a freely suspended metallic island, *Nano Lett.* **10**, 615 (2010).
- [6] V. I. Kleshch, V. Porshyn, A. S. Orekhov, A. S. Orekhov, D. Lützenkirchen-Hecht, and A. N. Obraztsov, Carbon single-electron point source controlled by Coulomb blockade, *Carbon* **171**, 154 (2021).
- [7] T. Esat, N. Friedrich, F. S. Tautz, and R. Temirov, A standing molecule as a single-electron field emitter, *Nature (London)* **558**, 573 (2018).
- [8] M. J. Fransen, T. L. van Rooy, and P. Kruit, Field emission energy distributions from individual multiwalled carbon nanotubes, *Appl. Surf. Sci.* **146**, 312 (1999).
- [9] S. T. Purcell, P. Vincent, M. Rodriguez, C. Journet, S. Vignoli, D. Guillot, and A. Ayari, Evolution of the field-emission properties of individual multiwalled carbon nanotubes submitted to temperature and field treatments, *Chem. Vapor Depos.* **12**, 331 (2006).
- [10] R. Diehl, M. Choueib, S. Choubak, R. Martel, S. Perisanu, A. Ayari, P. Vincent, S. T. Purcell, and P. Poncharal, Narrow energy distributions of electrons emitted from clean graphene edges, *Phys. Rev. B* **102**, 035416 (2020).
- [11] K. Nagaoka, H. Fujii, K. Matsuda, M. Komaki, Y. Murata, C. Oshima, and T. Sakurai, Field emission spectroscopy from field-enhanced diffusion-growth nano-tips, *Appl. Surf. Sci.* **182**, 12 (2001).
- [12] V. T. Binh, S. T. Purcell, N. Garcia, and J. Doglioni, Field-Emission Electron-Spectroscopy of Single-Atom Tips, *Phys. Rev. Lett.* **69**, 2527 (1992).
- [13] S. T. Purcell, V. T. Binh, and R. Baptist, Nanoprotrusion model for field emission from integrated microtips, *J. Vac. Sci. Technol. B* **15**, 1666 (1997).
- [14] R. H. Fowler and L. Nordheim, Electron emission in intense electric fields, *Proc. R. Soc. London, Ser. A* **119**, 173 (1928).
- [15] R. D. Young, Theoretical total-energy distribution of field-emitted electrons, *Phys. Rev.* **113**, 110 (1959).
- [16] J. Y. Huang, S. Chen, Z. F. Ren, G. Chen, and M. S. Dresselhaus, Real-time observation of tubule formation from amorphous carbon nanowires under high-bias Joule heating, *Nano Lett.* **6**, 1699 (2006).

- [17] L. Z. Zhao, Y. Cheng, Q. B. Zhang, and M. S. Wang, Seamless interconnections of sp(2)-bonded carbon nanostructures via the crystallization of a bridging amorphous carbon joint, *Mater. Horiz.* **6**, 72 (2019).
- [18] D. V. Averin, A. N. Korotkov, and K. K. Likharev, Theory of single-electron charging of quantum-wells and dots, *Phys. Rev. B* **44**, 6199 (1991).
- [19] K. K. Likharev, Single-electron devices and their applications, *Proc. IEEE* **87**, 606 (1999).
- [20] S. Mingels, V. Porshyn, B. Bornmann, D. Lützenkirchen-Hecht, and G. Müller, Sensitive fast electron spectrometer in adjustable triode configuration with pulsed tunable laser for research on photo-induced field emission cathodes, *Rev. Sci. Instrum.* **86**, 043307 (2015).
- [21] M. E. Lin, R. P. Andres, and R. Reifenberger, Observation of the Discrete Electron-Energy States of an Individual Nanometer-Size Supported Gold Cluster, *Phys. Rev. Lett.* **67**, 477 (1991).
- [22] See Supplemental Material at <http://link.aps.org/supplemental/10.1103/PhysRevB.102.235437> for details on the energy spectra fitting.
- [23] L. P. Kouwenhoven, D. G. Austing, and S. Tarucha, Few-electron quantum dots, *Rep. Prog. Phys.* **64**, 701 (2001).
- [24] A. T. Johnson, L. P. Kouwenhoven, W. de Jong, N. C. van der Vaart, C. J. P. M. Harmans, and C. T. Foxon, Zero-Dimensional States and Single Electron Charging in Quantum Dots, *Phys. Rev. Lett.* **69**, 1592 (1992).
- [25] G. N. Fursev and D. V. Glazanov, Deviations from the Fowler-Nordheim theory and peculiarities of field electron emission from small-scale objects, *J. Vac. Sci. Technol. B* **16**, 910 (1998).
- [26] M. Buttiker, Coherent and sequential tunneling in series barriers, *IBM J. Res. Dev.* **32**, 63 (1988).
- [27] R. Frisenda and H. S. J. van der Zant, Transition from Strong to Weak Electronic Coupling in a Single-Molecule Junction, *Phys. Rev. Lett.* **117**, 126804 (2016).
- [28] V. Filip and H. Wong, Comparative study of resonant and sequential features in electron field emission from composite surfaces, *Thin Solid Films* **608**, 26 (2016).
- [29] H. Schoeller and G. Schon, Mesoscopic quantum transport - resonant-tunneling in the presence of a strong Coulomb interaction, *Phys. Rev. B* **50**, 18436 (1994).
- [30] C. Wagner, M. F. B. Green, P. Leinen, T. Deilmann, P. Kruger, M. Rohlfing, R. Temirov, and F. S. Tautz, Scanning Quantum Dot Microscopy, *Phys. Rev. Lett.* **115**, 026101 (2015).
- [31] A. Tafel, S. Meier, J. Ristein, and P. Hommelhoff, Femtosecond Laser-Induced Electron Emission from Nanodiamond-Coated Tungsten Needle Tips, *Phys. Rev. Lett.* **123**, 146802 (2019).
- [32] H. Yanagisawa, C. Hafner, P. Dona, M. Klockner, D. Leuenberger, T. Greber, M. Hengsberger, and J. Osterwalder, Optical Control of Field-Emission Sites by Femtosecond Laser Pulses, *Phys. Rev. Lett.* **103**, 257603 (2009).
- [33] A. Aboubacar, M. Dupont, J. Gardes, M. Laguna, M. Querrou, and L. P. S. Says, Electron-beams triggered by a laser-pulse of a few tens ns duration from silicon cathodes with array of tips in high-electric-field, *Nucl. Instrum. Methods Phys. Res., Sect. A* **340**, 74 (1994).
- [34] S. Hirayama, F. Watanabe, T. Takahashi, and T. Motooka, Field emission current from Si tip: ultra-fast time resolved measurements, *Surf. Sci.* **515**, 369 (2002).
- [35] H. W. Fink, W. Stocker, and H. Schmid, Holography with Low-Energy Electrons, *Phys. Rev. Lett.* **65**, 1204 (1990).
- [36] A. Feist, K. E. Echternkamp, J. Schauss, S. V. Yalunin, S. Schafer, and C. Ropers, Quantum coherent optical phase modulation in an ultrafast transmission electron microscope, *Nature (London)* **521**, 200 (2015).